

PAPER • OPEN ACCESS

A self-powered and broadband UV PIN photodiode employing a NiOx layer and a β -Ga₂O₃ heterojunction

To cite this article: Jose Manuel Taboada Vasquez *et al* 2023 *J. Phys. D: Appl. Phys.* **56** 065104

View the [article online](#) for updates and enhancements.

You may also like

- [Enhancement of the Oxygen Evolution Using a 21-nm-Thin c-Si Photoanode with a Nano-Pyramid Texture](#)
Min-Joon Park, Jong Heo, Hongsub Jee et al.
- [Electrocatalytic Oxidation of Methanol at Nanoparticle-Based MnOx/NiOx/Pt Ternary Catalysts: Optimization of Loading Level and Order of Deposition](#)
Ahmad M. Mohammad, Ghada H. El-Nowihy, Mostafa M. H. Khalil et al.
- [Synergistic Effect of Urea on Vitamin C Electro-Oxidation at NiOx/CoOx Binary Catalysts Supported on Graphene Nanosheets](#)
Ghada H. El-Nowihy and Mohamed S. El-Deab

ECS Toyota Young Investigator Fellowship

For young professionals and scholars pursuing research in batteries, fuel cells and hydrogen, and future sustainable technologies.

At least one \$50,000 fellowship is available annually.
More than \$1.4 million awarded since 2015!



Application deadline: January 31, 2023



TOYOTA

Learn more. Apply today!

A self-powered and broadband UV PIN photodiode employing a NiO_x layer and a β -Ga₂O₃ heterojunction

Jose Manuel Taboada Vasquez¹ , Aasim Ashai², Yi Lu¹, Vishal Khandelwal¹, Manoj Rajbhar¹, Mritunjay Kumar¹, Xiaohang Li^{1,*}  and Biplab Sarkar^{2,*} 

¹ Advanced Semiconductor Laboratory, King Abdullah University of Science and Technology, Thuwal 23955, Saudi Arabia

² Department of Electronics and Communication Engineering, Indian Institute of Technology, Roorkee, Uttarakhand 247667, India

E-mail: xiaohang.li@kaust.edu.sa and bsarkar@ece.iitr.ac.in

Received 19 September 2022, revised 29 November 2022

Accepted for publication 28 December 2022

Published 20 January 2023



Abstract

Crucial commercial and space applications require the detection of broadband ultraviolet (UV) rays spanning from UV-A to UV-C. In this study, the authors demonstrate a broadband UV photodetector employing a p-type NiO_x layer and an n-type β -Ga₂O₃ heterostructure in PIN configuration for the first time. Simulations are conducted to optimize the doping concentration and thickness of the NiO_x layer, ensuring that (a) a reasonable depletion width is maintained within the NiO_x layer for UV-A and UV-B light absorption; (b) anode ohmic contacts are formed on the nondepleted NiO_x film, and (c) >70% of the UV-C light is absorbed by β -Ga₂O₃. The optimized NiO_x/ β -Ga₂O₃ PIN photodiode exhibits good responsivity to incident light wavelengths in the UV-A, UV-B, and UV-C regions. While the NiO_x layer is considered to be responsible for providing good photoresponsivity in the UV-A and UV-B regions, a highly resistive (near-intrinsic) β -Ga₂O₃ layer is required for the absorption of incident UV-C light. A record detectivity of $>10^{11}$ cm Hz^{0.5} W⁻¹ for the UV-B and UV-C regions and $>10^{10}$ cm Hz^{0.5} W⁻¹ for the UV-A region is observed in the NiO_x/ β -Ga₂O₃ heterostructure PIN photodiode during the self-powered operation. The results presented in this study are promising and instigate device design strategies for (ultra)wide bandgap semiconductor-based broadband UV PIN photodetectors.

Keywords: PIN photodiode, β -Ga₂O₃, broadband photodetector, detectivity, TCAD

(Some figures may appear in colour only in the online journal)

1. Introduction

Ultraviolet (UV) photodetectors are core devices for multiple commercial and strategic applications such as ozone

layer monitoring, flame detection, and space communications [1, 2]. Some of these applications require the detection of broadband UV-light wavelengths [3]. For example, the environment is exposed to harmful broad-range UV radiation because of ozone layer degradation [4]. Likewise, UV flame detectors mandate a broadband UV light detection to attain compatibility in versatile applications. For instance, diesel oil flame produces UV light in the range of 300–330 nm, while electric arc consists of broadband UV light in the range of 200–400 nm [5–7]. Other applications, such as bioaerosol detection, nondestructive forensic examination and

* Authors to whom any correspondence should be addressed.



Original content from this work may be used under the terms of the [Creative Commons Attribution 4.0 licence](https://creativecommons.org/licenses/by/4.0/). Any further distribution of this work must maintain attribution to the author(s) and the title of the work, journal citation and DOI.

astronomical telemetry imaging systems require detectors with a broadband UV spectral response [8]. Wide bandgap semiconductors with a bandgap (E_g) of >3 eV are preferred for fabricating UV photodetectors to overcome the requirement of expensive filters [9]. Several wide bandgap semiconductors such as $\text{Mg}_{0.67}\text{Ni}_{0.77}\text{O}/\text{SrTiO}_3$ [10], perovskite single crystal [11], and $\text{AlGaIn}/\text{GaIn}$ [12] based photodiode has been reported to yield a broadband UV detectivity. While some of them are promising for commercialization, others pose challenges like production cost and reliability [13]. In recent years, $\beta\text{-Ga}_2\text{O}_3$ ($E_g \sim 4.8$ eV) has emerged as a potential candidate for developing UV photodetectors [13]. Single crystalline $\beta\text{-Ga}_2\text{O}_3$ wafers can be grown using low-cost bulk crystal growth methods. Moreover, $\beta\text{-Ga}_2\text{O}_3$ films offer an excellent thermal, chemical and mechanical stability at elevated temperatures [14]. However, standalone $\beta\text{-Ga}_2\text{O}_3$ photodiodes exhibit a sharp responsivity peak at ~ 250 nm, preventing them from detecting a broadband UV spectrum. Therefore, integrating $\beta\text{-Ga}_2\text{O}_3$ with a narrow bandgap semiconductor is essential for detecting a broadband UV spectrum.

In terms of the device design, most literature reports on $\beta\text{-Ga}_2\text{O}_3$ UV photodiodes are based on a P–N (hetero)junction [2, 4, 15] or a metal-semiconductor-metal (MSM) [16–18] configuration. Compared with the MSM configuration, P–N junction photodiodes have several advantages, such as lower dark current, higher responsivity, and better detectivity [9]. Furthermore, a considerable zero-bias built-in potential enables the self-powered operation of the P–N junction photodiode. Because of the nonavailability of p-type doping, $\beta\text{-Ga}_2\text{O}_3$ heterojunction photodiodes comprise an n-type $\beta\text{-Ga}_2\text{O}_3$ film and a suitable p-type oxide [19, 20] or a p-type semiconductor [9, 15]. In recent years, p-type NiO_x (E_g : 3.2–3.8 eV) has attracted considerable attention for complementing the n-type $\beta\text{-Ga}_2\text{O}_3$. NiO_x is a chemically stable and non-toxic oxide, providing a high visible light transmittance [19]. Furthermore, in several studies, good matching and a stable heterostructure between NiO_x and $\beta\text{-Ga}_2\text{O}_3$ films have been demonstrated [21, 22], as well as highly efficient $\text{NiO}_x/\beta\text{-Ga}_2\text{O}_3$ P–N junction diodes and Schottky barrier diodes have been demonstrated for power electronic applications [23–25].

A significant depletion region for light absorption in P–N junction photodiodes requires low epitaxial-film doping [26]. A P–N photodiode comprising a semiconductor heterojunction requires a reasonable depletion width for both semiconductors to achieve a broadband photoresponse [8]. Consequently, ohmic contacts in heterojunction P–N photodiodes are formed on low-doped films, particularly on the epitaxial film closer to the surface [8, 9]. Because the contact resistance is a strong function of the epitaxial-film doping [27, 28], P–N heterojunction photodiode ohmic contacts may suffer from a large-ohmic-contact resistance. However, PIN photodiodes provide a larger depletion region for light absorption without compromising the epitaxial-film doping near the ohmic contacts [29].

Nevertheless, although a $\text{NiO}_x/\beta\text{-Ga}_2\text{O}_3$ heterostructure provides broadband responsivity because of the bandgap difference, recent studies on $\text{NiO}_x/\beta\text{-Ga}_2\text{O}_3$ P–N junction

photodetectors demonstrate narrowband photoresponsivity characteristics in the 240–260 nm region [19, 30]. These observations can be primarily attributed to the non-optimization of the device design, i.e. optimum broadband UV characteristics require a reasonable depletion region in the NiO_x film to generate a photoresponse to incident UV-A and UV-B light. In contrast, the depletion region in $\beta\text{-Ga}_2\text{O}_3$ generates a photoresponse to incident UV-C light. Moreover, PIN configuration providing a larger depletion region for light absorption compared to the P–N junction has not been reported yet. This work reports a $\text{NiO}_x/\beta\text{-Ga}_2\text{O}_3$ PIN photodiode that exhibits a broadband UV detection capability for the first time. This feature is attributed to the overlapping of the photoresponsivity characteristics of NiO_x in the UV-A and UV-B spectra, and $\beta\text{-Ga}_2\text{O}_3$ in the UV-C spectrum. The proposed device exhibits a large photoresponse to incident light having a wavelength in the UV-A (360 nm), UV-B (300 nm), and UV-C (240 nm) spectra.

2. Experimental methods

Initially, device design optimization of the $\text{NiO}_x/\beta\text{-Ga}_2\text{O}_3$ PIN photodiode was conducted using the commercially available Silvaco Technology Computer Aided Design (TCAD) software. Parameters such as the bandgap and electron affinity of NiO_x and $\beta\text{-Ga}_2\text{O}_3$ were obtained from existing literature studies [19]. Next, quasi-vertical $\text{NiO}_x/\beta\text{-Ga}_2\text{O}_3$ PIN photodiodes were fabricated on commercially available $n^+\text{-Si}$ wafers. Figure 1(a) shows a schematic of the fabricated $\text{NiO}_x/\beta\text{-Ga}_2\text{O}_3$ PIN photodiode. All $\beta\text{-Ga}_2\text{O}_3$ films were deposited using the pulsed laser deposition (PLD) method, whereas the NiO_x film was deposited using a radio frequency sputtering system. Before PLD growth, Si wafers were cleaned using a piranha and buffer-oxide etch solution. The PLD deposition was conducted using 900 nm highly-doped $\beta\text{-Ga}_2\text{O}_3$ layers ($n^+\text{-Ga}_2\text{O}_3$), followed by a 100 nm low-doped $\beta\text{-Ga}_2\text{O}_3$ layer ($n^-\text{-Ga}_2\text{O}_3$) and then 100 nm highly-resistive (considered intrinsic) $\beta\text{-Ga}_2\text{O}_3$ films ($i\text{-Ga}_2\text{O}_3$). The PLD growth conditions were optimized to achieve doping concentrations of $\sim 10^{19}$ and $\sim 10^{17}$ cm^{-3} in the $n^+\text{-Ga}_2\text{O}_3$ and $n^-\text{-Ga}_2\text{O}_3$ films, respectively. Next, a 25 nm p-type NiO_x layer with a doping concentration of $\sim 10^{18}$ cm^{-3} was deposited. The dopant for Ga_2O_3 was SiO_2 , and for NiO_x was Li. Note that additional details on the growth process of PLD $\beta\text{-Ga}_2\text{O}_3$ and sputtered NiO_x films can be found in the literature [31–33]. The free carrier concentrations in the films were validated using Hall measurements. For this, Ga_2O_3 and NiO_x films were grown separately on different wafers, and Hall measurements were carried out on square-shaped samples using Van der Pauw geometry. Note that Si dopants in Ga_2O_3 are shallow, whereas Li dopants in NiO_x show an activation energy of ~ 110 meV [34]. Thus, the doping concentration in Ga_2O_3 was directly estimated from the Hall measurements, whereas the doping concentration in NiO_x was evaluated from the Hall measurement results.

The device fabrication started by exposing the $n^+\text{-Ga}_2\text{O}_3$ layer for contact formation. A hard mask was created to cover

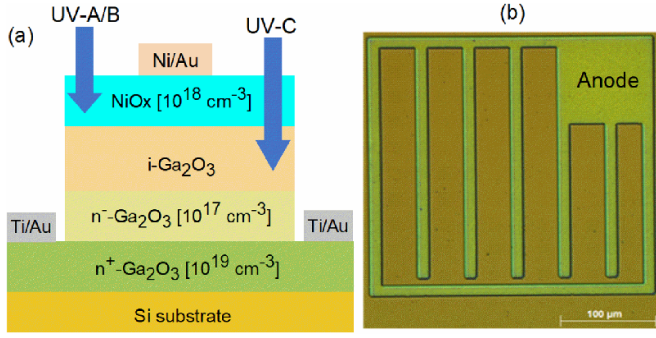


Figure 1. (a) Schematic of the fabricated NiO_x/β-Ga₂O₃ PIN photodiode; (b) micrograph (top view) of the photodiode.

a small area to enable cathode contact formation and deposition on the other side of n⁺-Ga₂O₃, i-Ga₂O₃, and NiO_x. A Ti/Au cathode ohmic contact was deposited on the exposed n⁺-Ga₂O₃ film. Similarly, Ni/Au anode ohmic contacts were deposited on NiO_x and patterned using conventional photolithography. Figure 1(b) shows the top view of the fabricated devices. Both metallization steps were implemented using the DC sputtering technique. The fabricated devices were annealed at 450 °C for 1 min to enable contact formation in a nitrogen atmosphere. The current–voltage (I–V) characteristics of the photodiodes were recorded using a Keithley 4200 semiconductor parameter analyzer. The photoresponsivity and pulse response of the photodiodes were measured using a test system (Zolix DSR600-x150-200-UV) supplied by Zolix Instruments Co., Ltd. This system includes a digital source meter (Keithley 2636B), a monochromator (TLS1509, Zolix), a Xe lamp, and a LabVIEW-developed software for measurement control. The system is capable of measuring photoresponsivity in the range of 200–1100 nm. All the measurements were performed at room temperature. Note that additional details on the photodiode characterization can be found in the literature [35, 36].

3. Results and discussion

A broadband UV response can be achieved when the optimum design of the photodiode device ensures that the depletion region in NiO_x results in a photoresponse to UV-A and UV-B light, whereas the depletion region in β-Ga₂O₃ results in a photoresponse to UV-C light, as shown in figure 1(a). Traditionally, the NiO_x layer exhibits broad UV absorption characteristics, having a peak absorption coefficient at ~310 nm [37]. However, the absorption coefficient of NiO_x for incident light with a wavelength of 250 nm is still a large quantity, indicating that a significant percentage of the incident light is absorbed within tens of nm of the NiO_x film thickness. The light absorption inside a semiconductor for a specific incident light wavelength is given as follows [38]:

$$\varphi = \varphi_0 e^{-\alpha x} \quad (1)$$

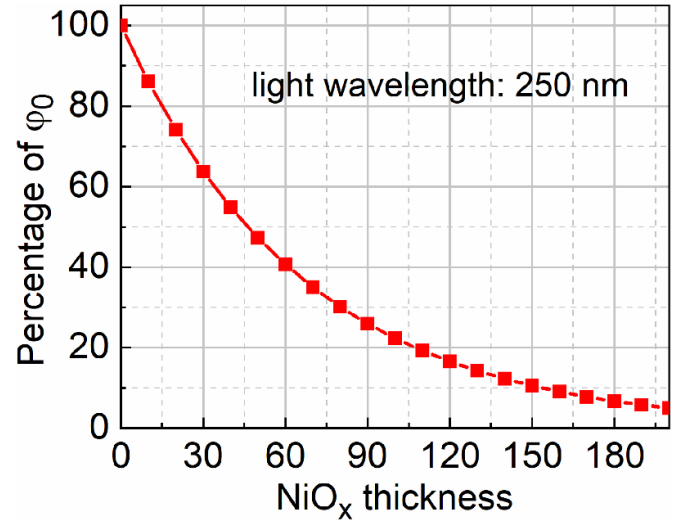


Figure 2. Percentage of the incident light intensity available in the NiO_x film as a function of the film thickness.

where φ is the light intensity available at a distance x from the NiO_x surface, φ_0 is the incident light intensity on the semiconductor (NiO_x in this case) surface, and α is the absorption coefficient at a specific wavelength [38]. Figure 2 shows the percentage of φ_0 (250 nm wavelength) in NiO_x for a given film thickness. It can be observed that only ~60% of the 250 nm wavelength incident light is available for absorption in β-Ga₂O₃ if the thickness of the NiO_x film is ~30 nm. Hence, for an optimum device design, the thickness of NiO_x film should be maintained at <30 nm.

TCAD simulations were conducted to optimize the NiO_x thickness and doping concentration. The aim was to ensure (a) a reasonable depletion region in the NiO_x film for UV-A and UV-B light absorption, and (b) nondepleted regions near the NiO_x surface to enable anode ohmic-contact formation with low contact resistance. The relation between the depletion region width and the doping across a heterojunction diode is given as follows [39]:

$$N_D x_n = N_A x_p \quad (2)$$

where N_D and N_A are the doping concentration in the n-type and p-type semiconductors, respectively, whereas x_n and x_p are the depletion width inside the n-type and p-type semiconductors. Equation (2) shows that the depletion region width strongly depends on the doping concentration across the heterojunction. The thickness of the depletion region inside the NiO_x film of the NiO_x/β-Ga₂O₃ PIN photodiode was observed to be ~19 nm for $N_A \sim 10^{18} \text{ cm}^{-3}$. Figure 3(b) shows the electric field profile inside the NiO_x/β-Ga₂O₃ PIN photodiode; ~6 nm of the NiO_x film was observed to be nondepleted. However, the thickness of the depletion region inside the NiO_x film of the NiO_x/β-Ga₂O₃ P–N junction photodiode is significantly larger than that of the PIN photodiode for a similar N_A , as shown in figure 3(c). To summarize, the NiO_x/β-Ga₂O₃ P–N junction photodiode requires a NiO_x film of <30 nm for

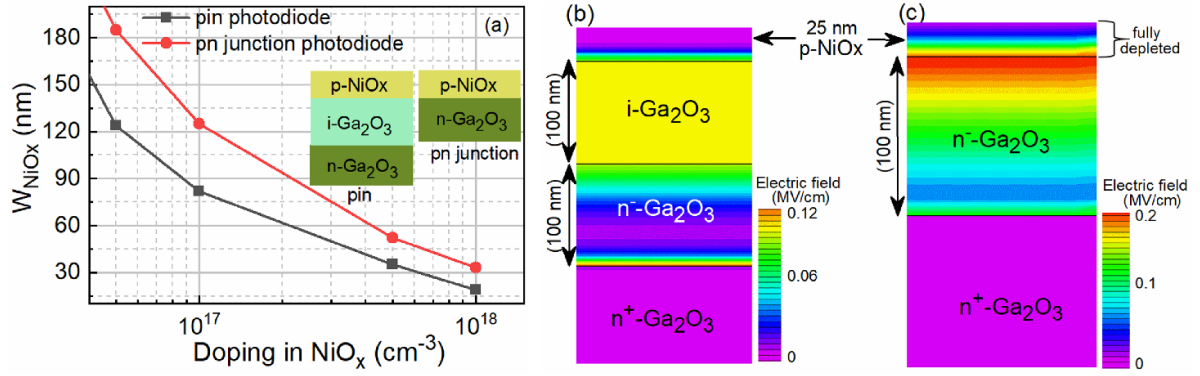


Figure 3. (a) Simulated thickness of the depletion region in NiO_x (W_{NiOx}) as a function of doping in the NiO_x film. Electric field profile inside NiO_x/β-Ga₂O₃: (b) PIN photodiode and (c) P–N junction photodiode. In (b) and (c), the doping concentrations are $N_A = 10^{18} \text{ cm}^{-3}$, $n^- = 10^{17} \text{ cm}^{-3}$, and $n^+ = 10^{19} \text{ cm}^{-3}$.

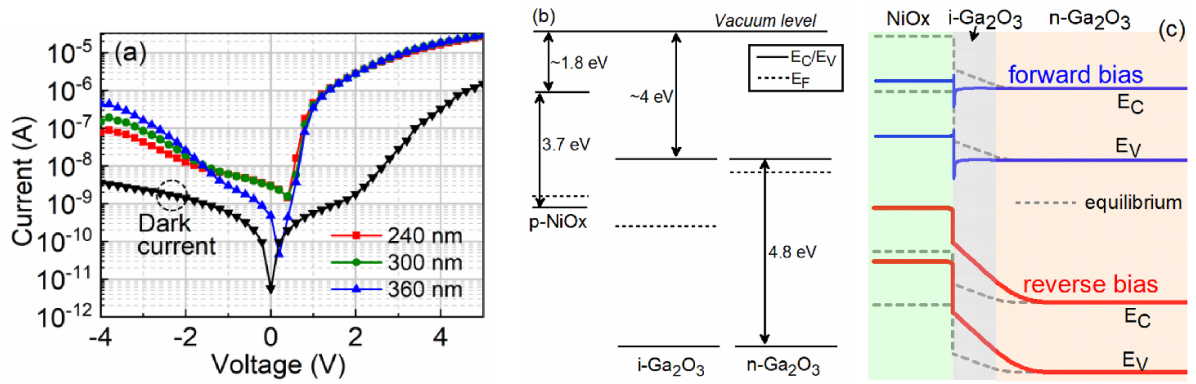


Figure 4. I–V characteristics of the NiO_x/β-Ga₂O₃ PIN photodiode under dark and illumination conditions; (b) energy band representation of individual NiO_x and Ga₂O₃ layers, and (c) energy band profile in equilibrium, forward bias and reverse bias.

$N_A \sim 10^{18} \text{ cm}^{-3}$ to ensure the formation of anode ohmic contacts on the nondepleted film. Moreover, the thickness of the depletion region for UV-C light absorption in the PIN photodiode is a user-defined quantity. The thickness of the intrinsic β-Ga₂O₃ film can vary by selecting appropriate growth conditions. The above observations indicate that a NiO_x/β-Ga₂O₃ photodiode in PIN configuration is advantageous over the currently popular P–N junction configuration. Figures 2 and 3(a) demonstrate that a NiO_x/β-Ga₂O₃ PIN photodiode comprising a 25 nm-thick NiO_x film and N_A of $\sim 10^{18} \text{ cm}^{-3}$ achieves (a) a reasonable thickness of the depletion region for UV-A and UV-B light absorption, (b) a nondepleted NiO_x film near the surface that enables ohmic-contact formation, and (c) >70% of the 250 nm wavelength incident light intensity available for absorption in the depletion regions of β-Ga₂O₃.

Next, the photoresponse of the NiO_x/β-Ga₂O₃ PIN photodiode was investigated by recording the I–V characteristics of the device under dark and illumination conditions for incident light wavelengths of 360, 300, and 240 nm, as shown in figure 4(a). Interestingly, the photoresponse in forward bias is observed to be higher than the reverse bias. To understand this, energy band diagram was investigated. Figure 4(b) shows the energy band profile of individual layers before the formation of NiO_x/β-Ga₂O₃ PIN photodiode. The energy band profile in forward bias and reverse bias is shown in figure 4(c). Forward

bias suppresses the potential barrier and depletion region leading to an enhanced charge carrier migration. On the contrary, promotion of the potential barrier and increased depletion region during reverse bias results in a restrained charge carrier migration. The enhanced photocurrent in forward bias is consistent with other literature reports on Ga₂O₃ based P–N heterojunction photodiodes [40]. However, forward bias minimizes the depletion region in NiO_x layer, indicating a compromised broadband detection during realistic device operation. Now, the photocurrent at zero bias is observed to be $>10^2$ higher than the dark current in the 240–360 nm range light wavelengths. An increase in the zero-bias current upon illumination confirms the self-powered operation of the photodiode. The photodiode quality was then investigated by evaluating the photoresponsivity (R_λ) and detectivity (D_λ), which are given as follows [4]:

$$R_\lambda = \frac{(I_{\text{photo}} - I_{\text{dark}})}{P \times A} \quad (3)$$

$$D_\lambda = \frac{R_\lambda}{\sqrt{2qJ_D}} \quad (4)$$

where I_{photo} is the photocurrent, I_{dark} is the dark current, P is the incident light intensity ($22 \mu\text{W cm}^{-2}$ in this work), A is

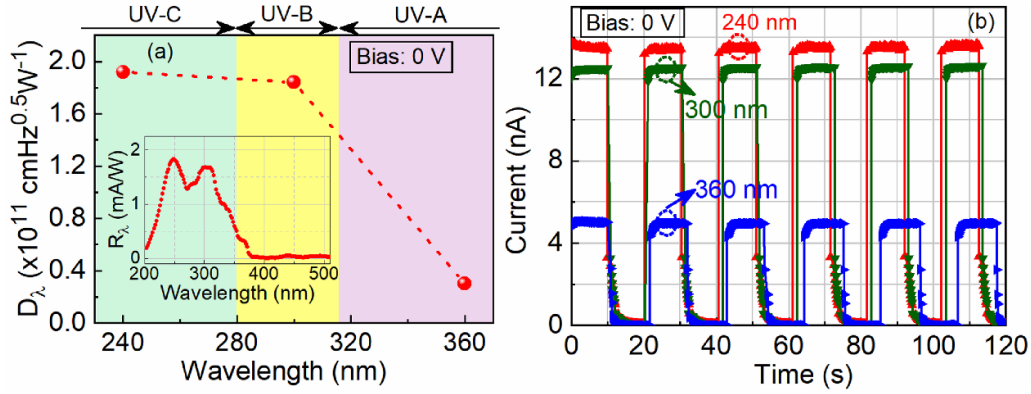


Figure 5. (a) Detectivity and (b) time response of the $\text{NiO}_x/\beta\text{-Ga}_2\text{O}_3$ PIN photodiode for incident light wavelengths of 240, 300, and 360 nm.

the effective area of the photodiode ($3.32 \times 10^{-4} \text{ cm}^2$), q is the electronic charge, and J_D is the dark-current density. The inset of figure 5(a) shows the R_λ of the $\text{NiO}_x/\beta\text{-Ga}_2\text{O}_3$ PIN photodiode at zero-bias voltage. It is observed that the overlapping of two distinct peaks results in broadband UV photoreponsivity. We speculate that the broader peak centered at $\sim 320 \text{ nm}$ is caused by the photoresponse of the depleted NiO_x film, whereas the photoresponse of the intrinsic $\beta\text{-Ga}_2\text{O}_3$ film causes the peak at $\sim 250 \text{ nm}$. Figure 5(a) shows the D_λ values of the photodiode for incident light wavelengths of 240, 300, and 360 nm. A record detectivity of $>10^{10} \text{ cm Hz}^{0.5} \text{ W}^{-1}$ is observed for the UV-A region, whereas the detectivity is $>10^{11} \text{ cm Hz}^{0.5} \text{ W}^{-1}$ for the UV-B and UV-C regions in the self-powered operation. The values of observed detectivities are summarized in table 1.

Next, figure 5(b) shows the time-dependent photoresponse of the photodetector for different incident light wavelengths. The time response was fitted to estimate the rise time (τ_r) and the decay time (τ_d) of the photodiode for a specific incident wavelength [19]. The τ_r (τ_d) values of the $\text{NiO}_x/\beta\text{-Ga}_2\text{O}_3$ PIN photodiode for incident light wavelengths of 360, 300, and 240 nm were reported to be 1.69 s (0.32 s), 0.87 s (0.44 s), and 0.71 s (0.65 s), respectively.

Finally, the performance of the broadband $\text{NiO}_x/\beta\text{-Ga}_2\text{O}_3$ UV PIN photodiode was benchmarked by comparing the proposed device with existing Ga_2O_3 -based heterojunction photodiodes reported in the literature, as shown in table 1. Most reports on self-powered broadband UV $\beta\text{-Ga}_2\text{O}_3$ photodiodes are based on the MSM or P–N junction configuration, as observed in table 1. Although the $\text{NiO}_x/\beta\text{-Ga}_2\text{O}_3$ heterostructure has been heavily investigated for power electronic applications, only a limited number of studies on the broadband capability of the $\text{NiO}_x/\beta\text{-Ga}_2\text{O}_3$ photodiode have been reported in the literature. For example, Wang *et al* [19] and Jia *et al* [30] fabricated $\text{NiO}_x/\beta\text{-Ga}_2\text{O}_3$ P–N junction photodiodes by maintaining a thick $\beta\text{-Ga}_2\text{O}_3$ layer on top of the NiO_x film. Significant photoresponsivity was observed only for a $\sim 250 \text{ nm}$ wavelength incident light with no noticeable/considerable photoresponse at longer wavelengths.

Similarly, Li *et al* [41] fabricated $\text{NiO}_x/\beta\text{-Ga}_2\text{O}_3$ P–N junction photodiodes by maintaining a 170 nm-thick NiO_x film

on top of the $\beta\text{-Ga}_2\text{O}_3$ film. These photodiodes exhibited a better detectivity of $2.27 \times 10^{11} \text{ cm Hz}^{0.5} \text{ W}^{-1}$ at a 7 V applied bias for an incident light wavelength of 260 nm. Presumably, the detectivity in the self-powered operation is possibly significantly lower. Furthermore, the work of Li *et al* [41] did not mention the broadband UV detection characteristics of the proposed photodiodes. Therefore, the detectivities observed in this study for $\text{NiO}_x/\beta\text{-Ga}_2\text{O}_3$ heterostructure based PIN photodiode during self-powered operation is a significant milestone, thanks to the device optimization performed using the TCAD simulations. In other studies on $\beta\text{-Ga}_2\text{O}_3$ -based broadband UV photodetectors, p-type semiconductors (GaN, GaSe, and CuOx) were used, as shown in table 1. However, the interface quality of the heterostructure between $\beta\text{-Ga}_2\text{O}_3$ and semiconductors, such as GaN, GaSe, and CuOx, is still unclear. The $\text{NiO}_x/\beta\text{-Ga}_2\text{O}_3$ photodiode investigated in this work exhibits reliable broadband characteristics and higher detectivity in the self-powered mode than other reported $\text{NiO}_x/\beta\text{-Ga}_2\text{O}_3$ P–N junction photodiodes. Moreover, as shown in table 1, lower doping in the p-type region (than that of the proposed device) was employed in existing studies on P–N junction broadband UV $\beta\text{-Ga}_2\text{O}_3$ photodiodes. Such low doping near the anode contact region possibly induces a large contact resistance and may hinder the commercialization process.

Next, we present a discussion to justify the importance of the proposed $\text{NiO}_x/\beta\text{-Ga}_2\text{O}_3$ broadband UV PIN photodiode. Bulk $\beta\text{-Ga}_2\text{O}_3$ single crystals are progressing fast to achieve commercial maturity because of the compatibility of $\beta\text{-Ga}_2\text{O}_3$ films with low-cost growth techniques such as the Czochralski growth method [14, 42]. To date, highly efficient kilovolt-class $\beta\text{-Ga}_2\text{O}_3$ Schottky diodes [43, 44] and P–N junction diodes [23, 45] have already been reported in the literature. These reports used single crystalline Ga_2O_3 substrates that are likely to offer better carrier mobility than the Ga_2O_3 films grown on Si substrate in this work. For instance, the mobility in low-doped Ga_2O_3 film was observed to be $\sim 10 \text{ cm}^2 \text{ V}^{-1} \text{ s}^{-1}$, much lower than single crystalline films for a similar doping concentration [42]. Moreover, Zhou *et al* reported a low trap density of $\sim 2.2 \times 10^{10} \text{ eV}^{-1} \text{ cm}^{-2}$ at the $\text{NiO}_x/\text{Ga}_2\text{O}_3$ interface [46]. Such a low trap density enables a high $I_{\text{on}}/I_{\text{off}}$ ratio of 10^6 (or more) in $\text{NiO}_x/\text{Ga}_2\text{O}_3$

Table 1. Benchmark table comparing recent studies on β -Ga₂O₃ heterojunction UV photodiodes.

Photodiode	Diode configuration	Wavelength range (nm)	Doping near contacts (cm ⁻³)	Detectivity ($\times 10^{11}$ cm Hz ^{0.5} W ⁻¹)	Responsivity (A/W)	t_r/t_d (s/s)	Reference
NiOx/Ga ₂ O ₃	PIN	240–360	P: 5×10^{17} N: 10^{19}	240 nm: 1.92 300 nm: 1.84 360 nm: 0.3	1.9×10^{-3} 1.7×10^{-3} 0.4×10^{-3}	0.71/0.65 0.87/0.44 1.69/0.32	This work
NiOx/Ga ₂ O ₃ ^a	P–N	245	Unknown	31.4 (10 V bias)	27.43 (10 V bias)	—	Jia <i>et al</i> [30]
NiO _x /Ga ₂ O ₃	P–N	254	Unknown	0.0545	57×10^{-6}	0.34/3.65	Wang <i>et al</i> [19]
NiO _x /Ga ₂ O ₃ ^a	P–N	260	Unknown	~0.628	0.362 (7 V bias)	—	Li <i>et al</i> [41]
GaN/Ga ₂ O ₃	P–N	256–365	P: 10^{15} N: 10^{15}	0.47	—	—	Kalra <i>et al</i> [8]
GaN/Ga ₂ O ₃	P–N	254–365	P: 6×10^{16} N: 10^{19}	254 nm: 0.617 365 nm: 1.23	28.44 54.43	0.14/0.07 0.1/0.08	Li <i>et al</i> [9]
CuOx/Ga ₂ O ₃ ^a	P–N	390–visible	P: unknown N: 2.7×10^{18}	390 nm: 5.2 (16 V bias)	53 (16 V bias)	0.2/0.2	Bae <i>et al</i> [2]
GaSe/Ga ₂ O ₃	P–N	254	Unknown	120	190	0.32 μ /52.6 μ	Wang <i>et al</i> [15]
SnO ₂ /Ga ₂ O ₃ ^a	MSM	254–302	P: unknown N: 6×10^{16}	254 nm: 17 000 (50 V bias) 302 nm: 2970 (50 V bias)	1532 (50 V bias) 262 (50 V bias)	0.2/3	Mondal <i>et al</i> [4]

^a Not a self-powered photodiode.

PN junction power diodes fabricated on single crystalline Ga₂O₃ substrates [25, 45], contrary to only $\sim 10^3$ observed in this work (see figure 4(a)). Therefore, it can be safely assumed that an improved performance (photoresponsivity and detectivity) can be attained by the proposed NiO_x/β-Ga₂O₃ PIN photodiode when implemented on single crystalline Ga₂O₃ substrates. Moreover, to our knowledge, there is no report on β-Ga₂O₃-based PIN diodes, which are important for both power electronic [47] and photodetector [48] applications. Regarding a P–N junction photodiode, a large depletion region, which is necessary for light absorption, requires low epitaxial-film doping. Unfortunately, the ohmic-contact resistance is an inverse function of the epitaxial-film doping near the contacts [28]. Consequently, P–N junction photodiodes possibly result in a significant contact resistance, as shown in figure 2(a). However, adding a highly resistive (near intrinsic) layer provides improved thickness optimization and a large depletion region, which is necessary for photodetection. Consequently, a highly doped epitaxial layer can be used for ohmic-contact formation in a PIN photodiode. However, TCAD simulations indicated that the absence of the intrinsic β-Ga₂O₃ layer, which is necessary to form a broadband NiO_x/β-Ga₂O₃ P–N junction photodiode, requires a thick NiO_x film to achieve a good anode-ohmic-contact formation. Alternatively, reducing the NiO_x thickness in a NiO_x/β-Ga₂O₃ P–N junction photodiode to achieve improved UV-C absorption would require an increase in NiOx doping, thus reducing the corresponding thickness of the depletion region and resulting in a compromised UV-A and UV-B absorption.

Finally, the switching speed of a photodiode is a function of the net depletion capacitance; a large thickness of the depletion region is required to achieve a fast response. The addition of an intrinsic region ensures a large and controllable thickness of

the depletion region. Unfortunately, in this work, the observed response time of the carriers is large, which is probably caused by the poor material quality. However, good quality epitaxial films are expected to yield a faster photoresponse in PIN configuration than the P–N junction configuration [49]. This involves the usage of suitable substrates, optimization of deposition techniques and thermal annealing processes. For instance, metalorganic chemical vapor deposition grown Ga₂O₃ films on foreign substrate yielded P–N junction photodiode response time in low- μ s range [15], contrary to hundreds of msec response time observed in this work on PLD Ga₂O₃ film counterpart. As mentioned previously, the NiOx/Ga₂O₃ interface plays a pivotal role in the overall performance of the photodiode. The charged defects (and the corresponding electric field) causes a considerable reduction in the photo-generated carrier velocity, thereby increasing the carrier transit time [50]. Finally, optimization of the intrinsic layer thickness is also important in improving the PIN photodiode response time. A thicker intrinsic layer offers a lower device capacitance, but increases the device resistance. Thus, the analysis and methods presented in this study are promising and instigate device design strategies for future broadband UV photodetectors based on (ultra)wide bandgap semiconductor heterostructures in PIN configuration.

4. Conclusion

This study proposed a broadband UV PIN photodiode based on a NiOx/β-Ga₂O₃ heterostructure. TCAD simulations were conducted to optimize the doping and thickness of NiO_x films to ensure (a) a reasonable thickness of the depletion region for UV-A and UV-B light absorption, (b) a nondepleted NiO_x film near the surface for ohmic-contact formation, and

(c) >70% of the 250 nm wavelength (UV-C) incident light intensity available for absorption in the depletion regions of β -Ga₂O₃. Consequently, the optimized NiO_x/β-Ga₂O₃ photodiode exhibited record detectivities of 1.92×10^{11} , 1.84×10^{11} , and 0.3×10^{11} cm Hz^{0.5} W⁻¹ for incident light wavelengths of 240, 300, and 360 nm, respectively. Finally, the analysis and methods presented in this paper are promising and instigate device design strategies for future broadband UV PIN photodetectors based on (ultra)wide bandgap semiconductor heterostructures.

Data availability statement

The data that support the findings of this study are available upon reasonable request from the authors.

Acknowledgments

The KAUST researchers are grateful for the funding support of Baseline Fund: BAS/1/1664-01-01, Near-term Grand Challenge Fund: REI/1/4999-01-01, and Impact Acceleration Fund: REI/1/5124-01-01.


Conflict of interest

The authors have no conflicts of interest to disclose.

Ethics approval

This article does not contain any studies performed by any of the authors that include humans or animals.

ORCID iDs

Jose Manuel Taboada Vasquez  <https://orcid.org/0000-0003-1710-2348>

Xiaohang Li  <https://orcid.org/0000-0002-4434-365X>

Biplab Sarkar  <https://orcid.org/0000-0003-0074-0626>

References

- [1] Mukhopadhyay S, Pal H, Narang S R, Guo C, Ye J, Guo W and Sarkar B 2021 Self-powered ultraviolet photodiode based on lateral polarity structure GaN films *J. Vac. Sci. Technol. B* **39** 052206
- [2] Bae H *et al* 2019 Solar-blind UV photodetector based on atomic layer-deposited Cu₂O and nanomembrane β-Ga₂O₃ pn oxide heterojunction *ACS Omega* **4** 20756–61
- [3] Li S *et al* 2021 Broadband ultraviolet self-powered photodetector constructed on exfoliated β-Ga₂O₃/CuI core-shell microwire heterojunction with superior reliability *J. Phys. Chem. Lett.* **12** 447–53
- [4] Mondal A, Nandi S, Yadav M K, Nandi A and Bag A 2022 Broad range (254–302 nm) and high performance Ga₂O₃: SnO₂ based deep UV photodetector *IEEE Trans. Nanotechnol.* **21** 320–7
- [5] Hidegh G and Józsa V 2020 Correlation analysis of chemiluminescent and pollutant emissions of a liquid-fueled turbulent swirl burner *J. Energy Inst.* **93** 1390–8
- [6] Nagi L, Koziol M and Zygarlicki J 2020 Optical radiation from an electric arc at different frequencies *Energies* **13** 1676
- [7] Okuno T, Ojima J and Saito H 2001 Ultraviolet radiation emitted by CO₂ arc welding *Ann. Occup. Hyg.* **45** 597–601
- [8] Kalra A, Vura S, Rathkanthiwar S, Muralidharan R, Raghavan S and Nath D N 2018 Demonstration of high-responsivity epitaxial β-Ga₂O₃/GaN metal-heterojunction-metal broadband UV-A/UV-C detector *Appl. Phys. Express* **11** 064101
- [9] Li P, Shi H, Chen K, Guo D, Cui W, Zhi Y, Wang S, Wu Z, Chen Z and Tang W 2017 Construction of GaN/Ga₂O₃ P–N junction for an extremely high responsivity self-powered UV photodetector *J. Mater. Chem. C* **5** 10562–70
- [10] Sarcan F, Orchard S, Kuerbanjiang B, Skeparovski A, Lazarov V K and Erol A 2020 Ultraviolet photodetector based on Mg_{0.67}Ni_{0.33}O thin film on SrTiO₃ *Phys. Status Solidi* **14** 2000175
- [11] Cheng Z, Liu K, Yang J, Chen X, Xie X, Li B, Zhang Z, Liu L, Shan C and Shen D 2019 High-performance planar-type ultraviolet photodetector based on high-quality CH₃NH₃PbCl₃ perovskite single crystals *ACS Appl. Mater. Interfaces* **11** 34144–50
- [12] Martens M, Schlegel J, Vogt P, Brunner F, Lossy R, Würfl J, Weyers M and Kneissl M 2011 High gain ultraviolet photodetectors based on AlGaN/GaN heterostructures for optical switching *Appl. Phys. Lett.* **98** 211114
- [13] Chen X, Ren F-F, Ye J and Gu S 2020 Gallium oxide-based solar-blind ultraviolet photodetectors *Semicond. Sci. Technol.* **35** 023001
- [14] Pearton S J, Yang J, Cary I V P H, Ren F, Kim J, Tadjer M J and Mastro M A 2018 A review of Ga₂O₃ materials, processing, and devices *Appl. Phys. Rev.* **5** 011301
- [15] Wang Y *et al* 2021 p-GaSe/n-Ga₂O₃ van der Waals heterostructure photodetector at solar-blind wavelengths with ultrahigh responsivity and detectivity *ACS Photonics* **8** 2256–64
- [16] Bae J, Jeon D-W, Park J-H and Kim J 2021 High responsivity solar-blind metal-semiconductor-metal photodetector based on α-Ga₂O₃ *J. Vac. Sci. Technol. A* **39** 033410
- [17] Arora K, Goel N, Kumar M and Kumar M 2018 Ultrahigh performance of self-powered β-Ga₂O₃ thin film solar-blind photodetector grown on cost-effective Si substrate using high-temperature seed layer *ACS Photonics* **5** 2391–401
- [18] Pratiyush A S, Krishnamoorthy S, Kumar S, Xia Z, Muralidharan R, Rajan S and Nath D N 2018 Demonstration of zero bias responsivity in MBE grown β-Ga₂O₃ lateral deep-UV photodetector *Jpn. J. Appl. Phys.* **57** 060313
- [19] Wang Y, Wu C, Guo D, Li P, Wang S, Liu A, Li C, Wu F and Tang W 2020 All-oxide NiO/Ga₂O₃ P–N junction for self-powered UV photodetector *ACS Appl. Electron. Mater.* **2** 2032–8
- [20] Watahiki T, Yuda Y, Furukawa A, Yamamuka M, Takiguchi Y and Miyajima S 2017 Heterojunction p-Cu₂O/n-Ga₂O₃ diode with high breakdown voltage *Appl. Phys. Lett.* **111** 222104
- [21] Zhang J, Han S, Cui M, Xu X, Li W, Xu H, Jin C, Gu M, Chen L and Zhang K H L 2020 Fabrication and interfacial electronic structure of wide bandgap NiO and Ga₂O₃ P–N heterojunction *ACS Appl. Electron. Mater.* **2** 456–63
- [22] Nakagomi S, Kubo S and Kokubun Y 2016 The orientational relationship between monoclinic β-Ga₂O₃ and cubic NiO *J. Cryst. Growth* **445** 73–77
- [23] Wang Y *et al* 2022 2.41 kV vertical P-NiO/n-Ga₂O₃ heterojunction diodes with a record Baliga's figure-of-merit of 5.18 GW/cm² *IEEE Trans. Power Electron.* **37** 3743–6
- [24] Gong H *et al* 2021 1.37 kV/12 A NiO/β-Ga₂O₃ heterojunction diode with nanosecond reverse recovery and rugged surge-current capability *IEEE Trans. Power Electron.* **36** 12213–7

- [25] Lu X, Zhou X, Jiang H, Ng K W, Chen Z, Pei Y, Lau K M and Wang G 2020 1-kV sputtered p-NiO/n-Ga₂O₃ heterojunction diodes with an ultra-low leakage current below 1 μ A/cm² *IEEE Electron Device Lett.* **41** 449–52
- [26] Murari K, Etienne-Cummings R, Thakor N and Cauwenberghs G 2009 Which photodiode to use: a comparison of CMOS-compatible structures *IEEE Sens. J.* **9** 752–60
- [27] Braslau N 1981 Alloyed ohmic contacts to GaAs *J. Vac. Sci. Technol.* **19** 803–7
- [28] Sarkar B, Reddy P, Klump A, Kaess F, Rounds R, Kirste R, Mita S, Kohn E, Collazo R and Sitar Z 2018 On Ni/Au alloyed contacts to Mg-doped GaN *J. Electron. Mater.* **47** 305–11
- [29] Zhang Y, Ma K, Zhao C, Hong W, Nie C, Qiu Z J and Wang S 2021 An ultrafast WSe₂ photodiode based on a lateral p-i-n homojunction *ACS Nano* **15** 4405–15
- [30] Jia M, Wang F, Tang L, Xiang J, Teng K S and Lau S P 2020 High-performance deep ultraviolet photodetector based on NiO/ β -Ga₂O₃ Heterojunction *Nanoscale Res. Lett.* **15** 47
- [31] Zhang F, Arita M, Wang X, Chen Z, Saito K, Tanaka T, Nishio M, Motooka T and Guo Q 2016 Toward controlling the carrier density of Si doped Ga₂O₃ films by pulsed laser deposition *Appl. Phys. Lett.* **109** 102105
- [32] Li J-S, Chiang C-C, Xia X, Yoo T J, Ren F, Kim H and Pearton S J 2022 Demonstration of 4.7 kV breakdown voltage in NiO/ β -Ga₂O₃ vertical rectifiers *Appl. Phys. Lett.* **121** 042105
- [33] Gong H H, Chen X H, Xu Y, Ren -F-F, Gu S L and Ye J D 2020 A 1.86-kV double-layered NiO/ β -Ga₂O₃ vertical P–N heterojunction diode *Appl. Phys. Lett.* **117** 022104
- [34] Dutta T, Gupta P, Gupta A and Narayan J 2010 Effect of Li doping in NiO thin films on its transparent and conducting properties and its application in heteroepitaxial P–N junctions *J. Appl. Phys.* **108** 083715
- [35] Lu Y, Krishna S, Tang X, Babatain W, Ben Hassine M, Liao C-H, Xiao N, Liu Z and Li X 2022 Ultrasensitive flexible κ -phase Ga₂O₃ solar-blind photodetector *ACS Appl. Mater. Interfaces* **14** 34844–54
- [36] Tang X et al 2022 Quasi-epitaxial growth of β -Ga₂O₃-Coated wide band gap semiconductor tape for flexible UV photodetectors *ACS Appl. Mater. Interfaces* **14** 1304–14
- [37] Mrabet C, Ben Amor M, Boukhachem A, Amlouk M and Manoubi T 2016 Physical properties of La-doped NiO sprayed thin films for optoelectronic and sensor applications *Ceram. Int.* **42** 5963–78
- [38] Donati S 2020 *Photodetectors: Devices, Circuits and Applications* (New York: Wiley-IEEE Press)
- [39] Sze S M and Lee M-K 2012 *Semiconductor Devices: Physics and Technology* 3rd edn (New York: Wiley)
- [40] Li S et al 2019 Ultrasensitive, superhigh signal-to-noise ratio, self-powered solar-blind photodetector based on n-Ga₂O₃/p-CuSCN core-shell microwire heterojunction *ACS Appl. Mater. Interfaces* **11** 35105–14
- [41] Li K H, Alfaraj N, Kang C H, Braic L, Hedhili M N, Guo Z, Ng T K and Ooi B S 2019 Deep-ultraviolet photodetection using single-crystalline β -Ga₂O₃/NiO heterojunctions *ACS Appl. Mater. Interfaces* **11** 35095–104
- [42] Jadhav A, Lyle L A M, Xu Z, Das K K, Porter L M and Sarkar B 2021 Temperature dependence of barrier height inhomogeneity in β -Ga₂O₃ Schottky barrier diodes *J. Vac. Sci. Technol. B* **39** 040601
- [43] Zhou H et al 2019 High-performance vertical β -Ga₂O₃ Schottky barrier diode with implanted edge termination *IEEE Electron. Device Lett.* **40** 1788–91
- [44] Mukhopadhyay S, Lyle L A M, Pal H, Das K K, Porter L M and Sarkar B 2022 Evidence of thermionic emission in forward biased β -Ga₂O₃ Schottky diodes at Boltzmann doping limit *J. Appl. Phys.* **131** 025702
- [45] Zhang J et al 2022 Ultra-wide bandgap semiconductor Ga₂O₃ power diodes *Nat. Commun.* **13** 3900
- [46] Zhou F et al 2021 Over 1.8 GW/cm² beveled-mesa NiO/ β -Ga₂O₃ heterojunction diode with 800 V/10 A nanosecond switching capability *Appl. Phys. Lett.* **119** 262103
- [47] Han S, Yang S and Sheng K 2021 Conductivity modulation in vertical GaN PiN diode: evidence and impact *IEEE Electron. Device Lett.* **42** 300–3
- [48] Kalra A, Rathkanthiwar S, Muralidharan R, Raghavan S and Nath D N 2019 Polarization-graded AlGaIn solar-blind p-i-n detector with 92% zero-bias external quantum efficiency *IEEE Photonics Technol. Lett.* **31** 1237–40
- [49] Decoster D and Harari J 2009 *Optoelectronic Sensors* (London: Wiley-ISTE Press)
- [50] Gity F, Hayes J M, Corbett B and Morrison A P 2011 Modeling the effects of interface traps on the static and dynamic characteristics of Ge/Si avalanche photodiodes *IEEE J. Quantum Electron.* **47** 849–57